Near field Rayleigh wave on soft porous layers

N. Geebelen, L. Boeckx,[a] G. Vermeir, and W. Lauriks
Laboratorium voor Akoestiek en Thermische Fysica, Katholieke Universiteit Leuven, Celestijnenlaan 200D, B-3001 Heverlee, Belgium

J. F. Allard and O. Dazel
Laboratoire d'Acoustique de l'Université du Maine, Avenue Olivier Messiaen, 72000 Le Mans, France

(Received 24 September 2007; revised 23 November 2007; accepted 12 December 2007)

Simulations performed for a typical semi-infinite reticulated plastic foam saturated by air show that, at distances less than three Rayleigh wavelengths from the area of mechanical excitation by a circular source, the normal frame velocity is close to the Rayleigh pole contribution. Simulated measurements show that a good order of magnitude estimate of the phase speed and damping can be obtained at small distances from the source. Simulations are also performed for layers of finite thickness, where the phase velocity and damping depend on frequency. They indicate that the normal frame velocity at small distances from the source is always close to the Rayleigh pole contribution and that a good order of magnitude estimate of the phase speed of the Rayleigh wave can be obtained at small distances from the source. Furthermore, simulations show that precise measurements of the damping of the Rayleigh wave need larger distances. Measurements performed on a layer of finite thickness confirm these trends. © *2008 Acoustical Society of America.*
[DOI: 10.1121/1.2832326]

PACS number(s): 43.20.Gp, 43.20.Jr, 43.20.Ye [LLT] Pages: 1241–1247

I. INTRODUCTION

Soft porous media like plastic foams and glass wools are widely used in room and building acoustics and by aircraft and car manufacturers as sound and vibration absorbers. Evaluating the rigidity coefficients at audio frequencies can be necessary to predict the performances of these materials, but most of the available methods solely allow measurements restricted to the quasistatic range.[1–4] It has been shown by Feng and Johnson that for a nondamped semi-infinite porous medium saturated by a light fluid and excited mechanically, the Rayleigh wave is the detectable surface mode.[5] In case of acoustical excitation, another type of surface wave will be dominant.[6] This wave is associated with the penetration of sound into the pores and is detectable by means of a microphone instead of a solid particle velocity sensor. Measuring the phase speed and damping of the Rayleigh wave in the audible frequency range can provide information concerning the rigidity coefficients. Some general properties of the frames of these media must be taken into account. The loss angle is large, around 1/10, and the velocity of the Rayleigh waves is around 50 m/s. The available porous samples have a finite thickness, generally around 2 cm, and measurements must be performed in the medium and the high frequency range to avoid strong finite thickness effects. Simulations have been performed previously with a short excitation in the time domain. It was shown by Allard *et al.*[7] that at a distance from the source large compared to the Rayleigh wavelength, for an ordinary damped soft medium saturated by air, the vertical deformation at the surface of the medium is mainly due to the contribution of the Rayleigh pole related to the elastic frame, slightly modified by the light saturating fluid. If this last property holds at small distances from the source, measurements at small distances of the source of the speed of the Rayleigh wave should be possible and easier than at large distances due to the large damping in most soft porous media. Moreover, measurements on small samples should be possible. Simulated measurements of the damping and the speed of the Rayleigh wave created by a circular source are performed in the time domain close to the source for a typical reticulated plastic foam. The relation between the simulated measurements of the speed and the damping of the Rayleigh wave and the phase speed and damping related to the Rayleigh pole at a given frequency is detailed, including the effects of finite layer thickness.

II. FRAME DISPLACEMENT INDUCED BY A SURFACE STRESS FIELD

The porous layer is represented in Fig. 1. It is in contact with air at the upper face. The layer is semi-infinite or has a finite thickness l. The layer with a finite thickness is bonded to an impervious rigid backing at the lower face. In this case the x and z displacement components of the frame and the z displacement component of the saturating air are equal to 0 at the lower face. Simulations have been performed for two normal stress fields with a time dependence $f(t)$. The true excitation is created by a small vibrating disc, with radius R, bonded onto the porous layer. Describing this excitation by means of a stress field is difficult. Instead of using a constant stress acting on a limited surface area $r<R$, an expression is used that will yield a fast and regular decreasing of its Hankel transform. The space dependence g_1 of the stress field acting on the frame at the air–porous layer interface is given by

[a]Electronic mail: laurens.boeckx@fys.kuleuven.be

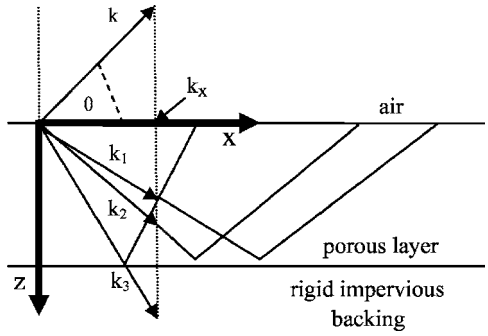

FIG. 1. The porous sample.

$$g_1(r) = (a_1/\pi)^{1/2} \exp(-a_1 r^2), \tag{1}$$

where r is the radial distance from the origin. The total force acting on the surface area $r<r_0$ is equal to $[1-\exp(-a_1 r_0^2)] \times(\pi/a_1)^{1/2}$ and the main contribution of the stress field is localized on the surface area $r<2a_1^{1/2}$. In a first step the Biot theory,[8] with the formalism developed in Ref. 9, is used to predict the vertical displacement u_z^s of the frame at the air–porous layer interface created by a stress field $\sigma_{zz} = \exp(ik_x x - i\omega t)$ acting on the frame at the surface of the layer. The plane waves that can propagate in a porous layer bonded to a rigid impervious backing are described in Ref. 10. The model by Johnson *et al.*[11] is used to describe the viscous and the inertial interactions and the model by Lafarge[12] is used for the bulk modulus of the saturating air. Let k_1 and k_2 be the wave numbers of the two Biot compressional waves and k_3 the wave number of the Biot shear wave. Let $\varphi_j^{\pm}$, $j=1,2$, be the velocity potentials of the compressional waves with the related displacement $\mathbf{u}^s = i\nabla\varphi\omega$. $\mathbf{\Psi}^{\pm} = \mathbf{n}\varphi_3^{\pm}$ are the velocity potentials of the shear waves, $\mathbf{n}$ being the unit vector on the y axis, with the related frame displacement $\mathbf{u}^s = i\nabla\wedge\mathbf{\Psi}/\omega$. The functions $\varphi_j^{\pm}$ can be written as

$$\varphi_j^{\pm} = a_j^{\pm} \exp(\pm i\alpha_j z + i\xi x), \quad j = 1,2,3, \tag{2}$$

$$\alpha_j = (k_j^2 - \xi^2)^{1/2}. \tag{3}$$

Three frame displacement fields $\mathbf{b}_1$, $\mathbf{b}_2$, and $\mathbf{b}_3$ are defined in Ref. 10 by the relations

$$\mathbf{b}_1 = \frac{i}{\omega}[\nabla(\exp(i\alpha_1 z) + r_{1,1}\exp(-i\alpha_1 z) + r_{1,2} \times\exp(-i\alpha_2 z)) + \nabla\wedge\mathbf{n}r_{1,3}\exp(-i\alpha_3 z)], \tag{4}$$

$$\mathbf{b}_2 = \frac{i}{\omega}[\nabla(r_{2,1}\exp(-i\alpha_1 z) + \exp(i\alpha_2 z) + r_{2,2} \times\exp(-i\alpha_2 z)) + \nabla\wedge\mathbf{n}r_{2,3}\exp(-i\alpha_3 z)], \tag{5}$$

$$\mathbf{b}_3 = \frac{i}{\omega}[\nabla(r_{3,1}\exp(-i\alpha_1 z) + r_{3,2}\exp(-i\alpha_2 z)) + \nabla\wedge\mathbf{n}(\exp(i\alpha_3 z) + r_{3,3}\exp(-i\alpha_3 z))]. \tag{6}$$

The coefficients r_{ij} are chosen so that each $\mathbf{b}_i$ satisfies the boundary conditions at the lower face. For a semi-infinite layer, the parameters r_{ij} are equal to 0. Let σ_{ij}^f be the stress components of the air in the porous medium and let σ_{ij}^s be the stress components of the frame. These stress components are related to forces per unit area of porous medium. At the upper face, the boundary conditions can be written, the common factor $\exp(ik_x x - i\omega t)$ being removed,

$$\phi\dot{u}_z^f + (1-\phi)\dot{u}_z^s = v_z, \tag{7}$$

$$\sigma_{zz}^f = -\phi p, \tag{8}$$

$$\sigma_{zz}^s = 1 - (1-\phi)p, \tag{9}$$

$$\sigma_{xz}^s = 0, \tag{10}$$

where ϕ is the porosity of the porous medium, $\dot{u}_z^f$ and $\dot{u}_z^s$ are the z components of the velocity of the saturating air and of the frame at the air–porous layer interface, p is the pressure, and v_z is the z velocity component in the free air close to the boundary. The pressure p and the velocity component v_z are related to a wave created in the free air at the boundary with a spatial dependence $\exp[i(xk_x - zk\cos\theta)]$, where k is the wave number in the free air. They satisfy the relation

$$v_z = -Zp/\cos\theta, \tag{11}$$

where Z is the characteristic impedance of air and θ is defined by $\sin\theta = k_x/k$. Using Eq. (11), p and v_z can be removed from the set of equations (7)–(9) that becomes

$$\sigma_{zz}^s - \frac{1-\phi}{\phi}\sigma_{zz}^f = 1, \tag{12}$$

$$(\phi\dot{u}_z^f + (1-\phi)\dot{u}_z^s) - \frac{Z}{\cos\theta}\frac{\sigma_{zz}^f}{\phi} = 0. \tag{13}$$

The frame displacement field in the porous medium is the sum $\lambda_1\mathbf{b}_1 + \lambda_2\mathbf{b}_2 + \lambda_3\mathbf{b}_3$ that satisfies Eqs. (10), (12), and (13). In Ref. 10, σ_{xy}^s, $\dot{u}_z^s$, $\dot{u}_z^f$, σ_{zz}^f, and σ_{zz}^s are given in Eqs. (A1)–(A5) by

$$\sigma_{xy}^s = M_{11}\lambda_1 + M_{12}\lambda_2 + M_{13}\lambda_{33}, \tag{14}$$

$$\dot{u}_z^s = M_{21}\lambda_1 + M_{22}\lambda_2 + M_{23}\lambda_3, \tag{15}$$

$$\dot{u}_z^f = M_{31}\lambda_1 + M_{32}\lambda_2 + M_{33}\lambda_3, \tag{16}$$

$$\sigma_{zz}^f = M_{41}\lambda_1 + M_{42}\lambda_2 + M_{43}\lambda_3, \tag{17}$$

$$\sigma_{zz}^s = M_{51}\lambda_1 + M_{52}\lambda_2 + M_{53}\lambda_3. \tag{18}$$

The following expressions for λ_1, λ_2, λ_3 are obtained:

$$\lambda_1 = \frac{B_2 M_{13} - B_3 M_{12}}{\Delta}, \tag{19}$$

$$\lambda_2 = \frac{B_3 M_{11} - B_1 M_{13}}{\Delta}, \tag{20}$$

$$\lambda_3 = \frac{B_1 M_{12} - B_2 M_{11}}{\Delta}, \tag{21}$$

where B_i, A_i, $i=1,2,3$, are given by

$$B_i = \phi M_{3i} + (1-\phi)M_{2i} - \frac{Z}{\cos\theta}\frac{M_{4i}}{\phi}, \tag{22}$$

$$A_i = M_{5i} - \frac{1-\phi}{\phi}M_{4i}, \tag{23}$$

$$\Delta = \begin{bmatrix} A_1 & A_2 & A_3 \\ B_1 & B_2 & B_3 \\ M_{11} & M_{12} & M_{13} \end{bmatrix}. \tag{24}$$

The z component of the frame velocity is given by Eq. (15) where λ_1, λ_2, λ_3 are given by Eqs. (19)–(21). The Hankel transform $\hat{g}_1$ of g_1 is given by

$$\hat{g}_1(k_r) = \int_0^\infty r g_1(r) J_0(k_r r) dr \tag{25}$$

and the z component of the frame velocity $v(r,t)$ at r is given by

$$v(r,t) = \frac{1}{2\pi}\int_{-\infty}^{\infty} d\omega \int_0^\infty dk_r \times \exp(-i\omega t) k_r \hat{g}_1(k_r) J_0(k_r r) \dot{u}(k_r). \tag{26}$$

Using $J_0(u) = 0.5[H_0^{(1)}(u) - H_0^{(1)}(e^{i\pi}u)]$ (Ref. 13, Chap. 9) and $\dot{u}(k_r) = \dot{u}(-k_r)$, Eq. (26) can be rewritten

$$v(r,t) = \frac{1}{4\pi}\int_{-\infty}^{\infty} d\omega \int_{-\infty}^{\infty} dk_r \exp(-i\omega t) k_r \hat{g}_1(k_r) H_0^{(1)} \times (k_r r)\dot{u}(k_r). \tag{27}$$

The function $\hat{g}_1$ is given by

$$\hat{g}_1(k_r) = \exp\left(\frac{-k_r^2}{4a_1}\right)/(2\sqrt{\pi a_1}). \tag{28}$$

A zero of the determinant Δ at $k_x = k_p$ corresponds to a pole of v at $k_r = k_p$, the contribution of the pole residue for v in Eq. (27) is given by

$$v_p(r,t) = \frac{i}{2}\int_{-\infty}^{\infty} d\omega \exp(-i\omega t) k_p \hat{g}_1(k_p) H_0^{(1)}(k_p r) R(k_p). \tag{29}$$

In Eq. (29), $R(k_p)$ is given by

$$R(k_p) = M_{21}\frac{B_2 M_{13} - B_3 M_{12}}{[\partial\Delta(k_x)/\partial k_x]_{k_x=k_p}} + M_{22}\frac{B_3 M_{11} - B_1 M_{13}}{[\partial\Delta(k_x)/\partial k_x]_{k_x=k_p}} + M_{23}\frac{B_1 M_{12} - B_2 M_{11}}{[\partial\Delta(k_x)/\partial k_x]_{k_x=k_p}}. \tag{30}$$

Another spatial dependence, $g_2(x)$, has been considered for the stress field source, given by

$$g_2(x) = \cos a_2 x, \quad 0 < |x| < \frac{\pi}{2a_2} \tag{31}$$

with $a_2 = 250\pi$. Using the double Fourier transform

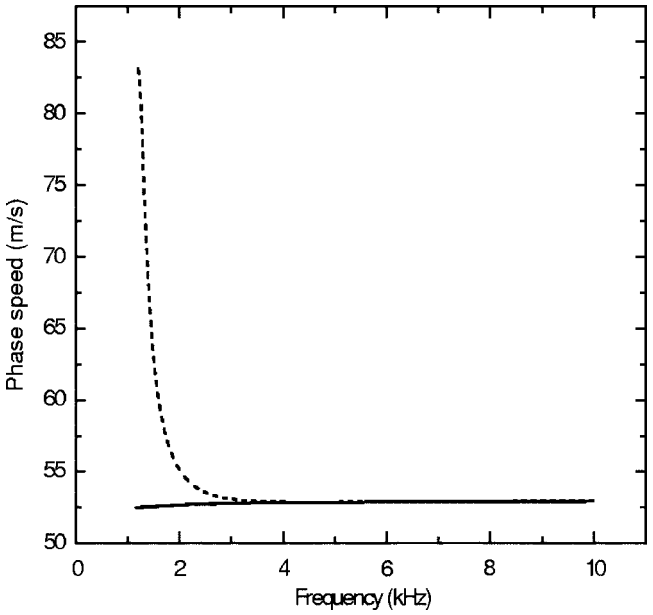

FIG. 2. Phase speed $\omega/\mathrm{Re}\,k_p$ of the modified Rayleigh wave, parameters of Table I, semi-infinite layer (—), thickness $l=2$ cm (- - -).

$$\tilde{g}_2(k_x)\tilde{f}(\omega)\int_{-\infty}^{\infty}\int_{-\infty}^{\infty} dt dx \exp(i\omega t - ik_x x) g_2(x) f(t), \tag{32}$$

the z component of the frame velocity at the surface of the porous medium is given by

$$v(x) = (2\pi)^{-2}\int_{-\infty}^{\infty}\int_{-\infty}^{\infty} d\omega dk_x \times \exp(-i\omega t + ik_x x)\tilde{g}_2(k_x)\tilde{f}(\omega)\dot{u}_z^s(k_x). \tag{33}$$

The function $\tilde{g}_2$ is given by

$$\tilde{g}_2(k_x) = \frac{2a_1}{a_1^2 - k_x^2}\cos\frac{\pi k_x}{2a_1}. \tag{34}$$

The contribution of the pole residue for v is given by

$$v_p(x,t) = \frac{i}{2\pi}\int_{-\infty}^{\infty} d\omega \times \exp(-i\omega t + ik_p x)\tilde{g}_2(k_p)\tilde{f}(\omega)\dot{u}_z^s(k_p)R(k_p). \tag{35}$$

III. SIMULATIONS

A. Rayleigh pole

The Rayleigh pole is located at $k_x = k_p$ where $\dot{u}_z^s$ is infinite. The wave number component k_p is obtained by an iterative method which minimizes $1/\dot{u}_z^s$ as a function of k_x. The initial value of k_x is the wave number of the Biot shear wave. The quantity $\omega/\mathrm{Re}\,k_p$, which is the phase speed of the Rayleigh wave, is represented in Fig. 2 for a layer of the medium of Table I similar to current reticulated plastic foams with a semi-infinite thickness and a thickness $l=2$ cm, as a function of frequency, and $\mathrm{Im}\,k_p$ is represented in Fig. 3. There is a strong finite thickness effect at frequencies lower than 2 kHz. At higher frequencies, k_p is not noticeably modified by the finite thickness.

TABLE I. Parameters for the porous material.

Porosity ϕ (—)	0.99
Flow resistivity σ (N m^{-4} s)	12 000
Thermal permeability k_0' (m^2)	1.5×10^{-9}
Viscous dimension Λ (μm)	100
Thermal dimension Λ' (μm)	400
Tortuosity α_∞ (—)	1.01
Density ρ_s (kg/m^3)	24.5
Shear modulus N (kPa)	$80(1+i/8)$
Poisson ratio [ν] (—)	0.3

B. Frame velocity

Simulations have been performed of the frame velocity resulting from a normal stress field $g_1(r)$ with a time dependence $f(t)$ and with the porous medium described in Table I. The time dependence $f(t)$ is the product of a sine function at different frequencies and a Blackman–Harris window with a duration equal to ten periods. The integration in ω in Eq. (27) is replaced by a fast Fourier transform. For the spatial dependencies g_1 of the excitation, $a_1=1.725\times10^5$. The integral in k_x in Eq. (27) is performed on the real axis in the physical Riemann sheet of the complex k_r plane. If the porous layer is semi-infinite, the physical sheet is characterized by

$$\mathrm{Im}\cos\theta>0, \tag{36}$$

$$\mathrm{Im}\,\alpha_i>0,\quad i=1,2,3. \tag{37}$$

If the porous sample is semi-infinite, the initial path of integration can be replaced by the three cuts related to the three Biot waves and the cut related to the wave in air in the same sheet. The residues of the poles which are crossed when the initial path is modified must be added to the integral on the new path. The determinant Δ for a semi-infinite layer is a polynomial in k_x and there is a finite number of poles. If the porous sample has a finite thickness the three cuts related to the Biot waves disappear and the determinant Δ has an infinite number of roots. The three cuts are replaced by the contributions of an infinite number of poles. The transition between the semi-infinite thickness and the finite thickness is described by Tamir and Felsen[14] for electromagnetic waves in the presence of a dielectric slab. The z component of the velocity v of the porous frame as a function of time at $r=3$ cm calculated with Eq. (27) is represented in Fig. 4 for a semi-infinite layer and in Fig. 5 for a layer of thickness $l=2$ cm. The contribution v_p of the Rayleigh pole given by Eq. (29) is also represented in Figs. 4 and 5. The pole contribution is limited to the frequencies in the interval 0.8–10 kHz in Fig. 5. It was verified that the contribution of the frequencies out of this interval is negligible. The Ray-

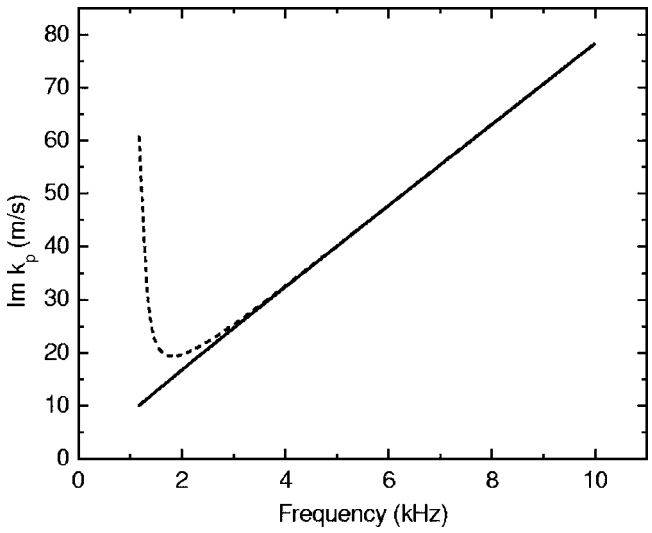

FIG. 3. Damping Im ξ_p of the modified Rayleigh wave, parameters of Table I, semi-infinite layer (—), thickness $l=2$ cm (- - -).

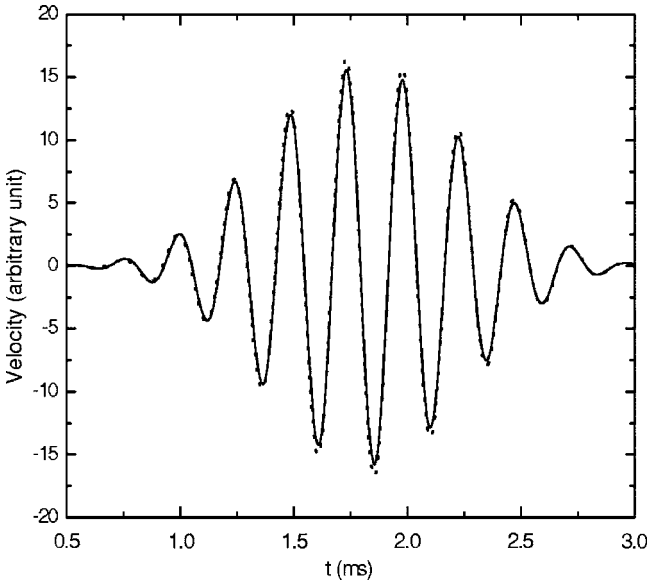

FIG. 4. Normal velocity v of the porous frame, semi-infinite layer, parameters of Table I, central frequency 4 kHz, circular source, $r=3$ cm, integral on the real k_r axis (—), pole contribution (- - -).

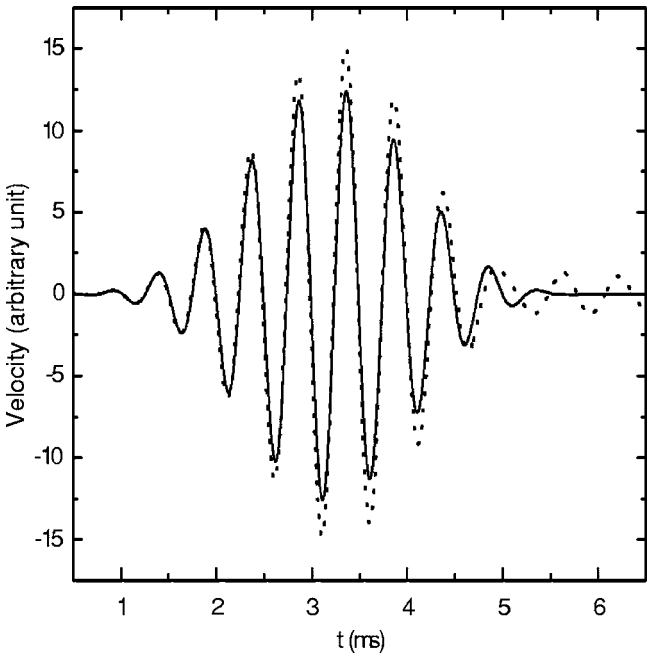

FIG. 5. Normal velocity v of the porous frame, thickness $l=2$ cm, parameters of Table I, central frequency 2 kHz, circular source, $r=3$ cm, integral on the real k_r axis (—), pole contribution (- - -).

TABLE II. Predicted $\omega/\mathrm{Re}\,k_r$ and $\mathrm{Im}\,k_r$ and simulated measurements of c_r and D at 4 kHz. Semi-infinite layer and finite thickness $l=5$ cm.

	$\omega/\mathrm{Re}\,k_p$ (m/s), c_r	$\mathrm{Im}\,k_p$ (m^{-1}), D
Prediction (semi-infinite layer) $\omega/\mathrm{Re}\,k_p$, $\mathrm{Im}\,k_p$	*52.8*	*32.4*
Simulation 3–4 cm pole c_r, D	52.6	32.5
Simulation 3–4 cm c_r, D	53.8	30.5
Simulation 15–16 cm pole c_r, D	53.2	32.0
Simulation 15–16 cm c_r,D	53.2	33.8
Simulation 3–5 cm $l=5$ cm c_r, D	53.2	36.1

leigh pole contribution is close to the total displacement in both cases, especially for the semi-infinite layer. Due to the fact that the contribution of the Rayleigh wave is dominant, an approximateevaluation of the speed and the damping of the Rayleigh wave should be possible at short distances from the source.

C. Simulated measurement of the speed and the damping of the Rayleigh wave

The intercorrelation function $I(\tau)$ given by

$$I(\tau)=\int f(t+\tau)v(r,t)dt \tag{38}$$

is successively predicted for a couple r_1, r_2 with $r_2>r_1$. Let I_1 and I_2 be the maxima of I at the distances r_1 and r_2, respectively, and let τ_1 and τ_2 be the related time lags. The speed c_r is evaluated by

$$c_r=(r_2-r_1)/(\tau_2-\tau_1). \tag{39}$$

Using the asymptotic expression of the Hankel function (Ref. 13, Chap. 9)

$$H_0^{(1)}(i)=\left(\frac{2}{\pi u}\right)^{1/2}\exp[i(u-\pi/4)], \tag{40}$$

the damping D is evaluated by

$$D=\frac{1}{r_2-r_1}\log\left(\sqrt{\frac{r_1}{r_2}}I_1/I_2\right). \tag{41}$$

The simulated measurements of c_r and D at the center frequency 4 kHz of the excitation are compared with the phase speed $\omega/\mathrm{Re}\,k_p$ and $\mathrm{Im}\,k_p$ at the same frequency in Table II for the semi-infinite layer. The simulated measurements are performed for the couple $r_1=3$ cm, $r_2=4$ cm and the couple $r_1=15$ cm, $r_2=16$ cm. In Eq. (38), I is successively evaluated with v and with v_p. The predicted values of the speeds c_r and $\omega/\mathrm{Re}\,k_p$ and of D and $\mathrm{Im}\,k_p$, respectively, are close to each other for both couples r_1, r_2. They are closer for the pole contribution than for the full contribution, and slightly closer for the couple 15–16 cm than for the couple 3–4 cm. This shows that for the chosen time dependence of the excitation at a given center frequency the Rayleigh wave speed and damping are close to the phase speed and $\mathrm{Im}\,k_p$ at the same frequency. The comparisons also show that the limitation in the precision of the evaluation is mainly due to the contributions of the cuts which decrease faster than the contribution of the pole with the distance. Simulations performed at 4 kHz for a layer of thickness $l=5$ cm present the same trends as for the semi-infinite layer. In Table III, the simulated measurements of the speed c_r and the damping D are compared with the predicted phase speeds $\omega/\mathrm{Re}\,k_p$ and $\mathrm{Im}\,k_p$ modified by the finite thickness $l=2$ cm, for the central frequencies 2, 3, and 4 kHz. The predicted values of the speeds are close to each other with a precision better than 10/100. The simulated measurement of D can be very different from $\mathrm{Im}\,k_p$. At 4 kHz, a simulated measurement of c_r and D is performed where the full evaluation of v_z is replaced by the pole contribution. With v_2 restricted to the pole contribution, in the last line of Table III, the quantities c_r and $\omega/\mathrm{Re}\,k_p$, and D and $\mathrm{Im}\,k_p$, respectively, are close to each other. This shows that the differences between D and $\mathrm{Im}\,k_p$ when the full evaluation of v is performed with Eq. (27) is not due to the dispersion of $\mathrm{Im}\,k_p$ but to the contribution of the other poles of $\dot{u}_z$. The fluctuation in amplitude due to the contribution of the other poles is much lower than the variation due to the damping when the difference r_2-r_1 is sufficiently large. This allows more precise measurements of $\mathrm{Im}\,k_p$ via the measurement of D by using larger distances r_2-r_1. The simulated measurements of D given in Table III for the couple $r_1=3$ cm, $r_2=10$ cm are close to the predicted $\mathrm{Im}\,k_p$ with an error smaller than 20/100.

TABLE III. Predicted $\omega/\mathrm{Re}\,k_p$ and $\mathrm{Im}\,k_p$ and simulated measurements of c_r and D, $l=2$ cm.

	$\omega/\mathrm{Re}\,k_p$ (m/s), c_r	$\mathrm{Im}\,k_p$(m^{-1}), D
Prediction 2 kHz $\omega/\mathrm{Re}\,k_p$, $\mathrm{Im}\,k_p$	*55.1*	*19.7*
Simulation 2 kHz, 3–4 cm c_r, D	55.5	17.2
Simulation 2 kHz, 4–5 cm c_r, D	54.3	18.9
Simulation 2 kHz, 3–10 cm c_r, D	52.4	21.6
Prediction 3 kHz $\omega/\mathrm{Re}\,k_p$, $\mathrm{Im}\,k_p$	*53.1*	*25.4*
Simulation 3 kHz, 3–4 cm c_r, D	53.2	5.2
Simulation 3 kHz, 4–5 cm c_r, D	56.0	8.4
Simulation 3 kHz, 3–10 cm c_r, D	52.4	21.6
Prediction 4 kHz $\omega/\mathrm{Re}\,k_p$, $\mathrm{Im}\,k_p$	*52.9*	*32.8*
Simulation 4 kHz, 3–4 cmc_r, D	47.7	25.8
Simulation 4 kHz, 4–5 cm c_r, D	58.1	7.2
Simulation 4 kHz, 3–10 cm c_r, D	53.4	31.5
Simulation 4 kHz, 3–4 cm, pole c_r, D	53.2	32.6

The same study has been performed with the geometry g_2 of the source. The results are very similar and are not reported.

IV. MEASUREMENTS

Measurements have been performed on a layer of thickness $l=2$ cm of a urethane foam. The surface area of the sample was 1.5×1.5 m^2, which is sufficiently large so that boundary effects do not affect the measurement of the Rayleigh wave velocity. For a melamine foam, it was even verified experimentally that the sample size could be reduced to 15×15 cm^2 without compromising the Rayleigh wave velocity. To obtain a uniform boundary condition double-faced tape was used to glue the porous layer onto a rigid impervious backing. Rayleigh waves were excited by means of a magnetic transducer putting in motion a circular plate of di-

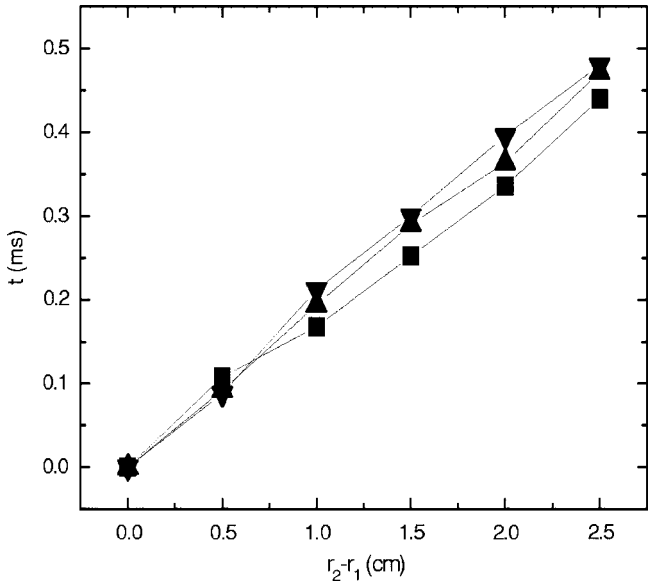

FIG. 6. Measured time $t=\tau_2-\tau_1$ vs displacement r_2-r_1, central frequency 2 kHz (■–■), 3 kHz (▼–▼), 3.5 kHz (▲–▲).

ameter 1 cm bonded on the layer. The magnetic transducer was consecutively fed with a sine burst signal of 2, 3, and 3.5 kHz, respectively. The time dependence of the signal is similar to the one in the modeling and the normal velocity of the frame is measured with a laser Doppler vibrometer. Measurement points are located on a radius through the excitation point. The radius was scanned up to 2.5 cm and with a typical step size of 5 mm. The damping D and the time of flight between two locations are evaluated from the intercorrelations like in the previous sections. The measured time of flight $t=\tau_2-\tau_1$ versus the distance r_2-r_1 is shown in Fig. 6 and the damping is shown in Fig. 7. The ratio $(r_2-r_1)/t$ is close to the speed 54 m/s with an order of magnitude of 10/100 for the dispersion. This result is in a reasonable agreement with measurements of the rigidity parameters of the same medium performed with a different method.[10] The

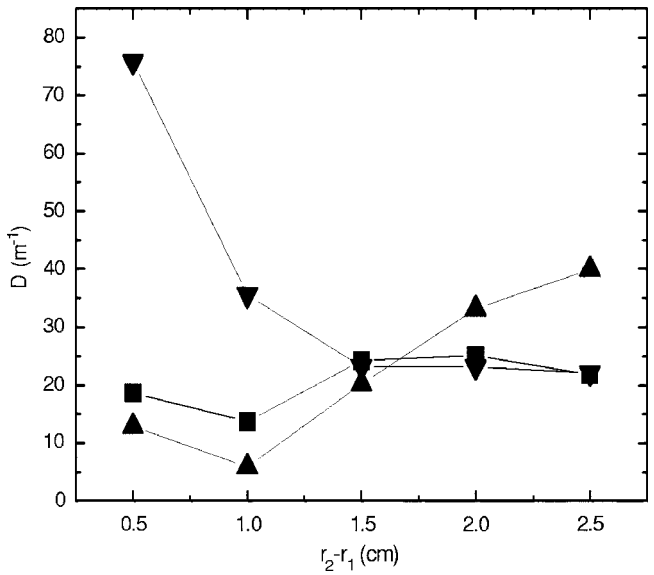

FIG. 7. Measured damping D, $r_1=3$ cm, central frequency 2 kHz (■–■), 3 kHz (▼–▼), 3.5 kHz (▲–▲).

evaluation of the speed of the Rayleigh wave can be performed at a small distance from the source but the measured damping at a given frequency presents a large dispersion and cannot be related to a precise Im k_p.

V. CONCLUSION

Predictions were performed in the frequency domain for soft and strongly damped porous media in contact with air. The wave number interface component of the pole of the Rayleigh plane wave was predicted as a function of frequency for a layer having a small thickness and a semi-infinite layer. The dependence of the phase velocity on the frequency due to the finite thickness was demonstrated. Simulations in the time domain were performed close to a circular source, showing that the residue related to the Rayleigh pole is the dominant contribution to the normal velocity of the frame for the semi-infinite layer and the layer of finite thickness. As a consequence, the speed of the Rayleigh wave and the damping can be evaluated at a small distance from the source for the semi-infinite layer, allowing an evaluation of the phase speed and the imaginary part of the Rayleigh pole. For the layer of finite thickness, the speed evaluation is also possible, but the contributions of the other poles create a fluctuation in the amplitude of the normal velocity which does not allow a precise evaluation of the damping at small distances from the source. Measurements are performed on a layer of small thickness. These measurements confirm that the evaluation of the speed is possible at small distances from the source.

ACKNOWLEDGMENT

L.B. is thankful for financial support obtained through a Research Mandatory of the Institute for the Promotion of Innovation through Science and Technology in Flanders (IWT-Vlaanderen).

[1]T. Pritz, "Measurement methods of complex Poisson's ratio of viscoelastic materials," Appl. Acoust. **60**, 279–292 (2000).
[2]M. Melon, M. Mariez, C. Ayrault, and S. Sahraoui, "Acoustical and mechanical characterization of anisotropie open-cell foams," J. Acoust. Soc. Am. **104**, 2622–2627 (1998).
[3]J. Park, "Measurement of the frame acoustic properties of porous and granular materials," J. Acoust. Soc. Am. **118**, 3483–3490 (2005).
[4]V. Tarnow, "Dynamic measurements of the elastic constants of glass wool," J. Acoust. Soc. Am. **118**, 3672–3678 (2005).
[5]S. Feng and D. L. Johnson, "High-frequency acoustic properties of a fluid/porous solid interface. I. New surface mode. II. The 2D reflection Green's function," J. Acoust. Soc. Am. **74**, 906–924 (1983).
[6]T. L. Richards and K. Attenborough, "Solid particle motion resulting from a point source above a poro-elastic half space," J. Acoust. Soc. Am. **86**, 1085–1092 (1989).
[7]J. F. Allard, G. Jansens, G. Vermeir, and W. Lauriks, "Frame-borne surface waves in air-saturated porous media," J. Acoust. Soc. Am. **111**, 690–696 (2002).
[8]M. A. Biot, "Theory of propagation of elastic waves in a fluid-saturated porous solid," J. Acoust. Soc. Am. **28**, 168–191 (1956).
[9]J. F. Allard, *Propagation of Sound in Porous Media, Modelling Sound Absorbing Materials* (Elsevier, London, 1993).
[10]J. F. Allard, B. Brouard, N. Atalla, and S. Ghinet, "Excitation of soft porous frames resonances and evaluation of the rigidity coefficients," J.

Acoust. Soc. Am. **121**, 78–84 (2007).
[11]D. L. Johnson, J. Koplik, and R. Dashen, "Theory of dynamic permeability and tortuosity in fluid-saturated porous media," J. Fluid Mech. **176**, 379–402 (1987).
[12]D. Lafarge, P. Lemarinier, J. F. Allard, and V. Tarnow, "Dynamic compressibility of air in porous structures at audible frequencies," J. Acoust. Soc. Am. **102**, 1995–2006 (1997).
[13]M. Abramovitz and I. A. Stegun, *Handbook of Mathematical Functions* (Dover, New York, 1970).
[14]T. Tamir and L. B. Felsen, "On lateral waves in slab configurations and their relation to other wave types," IEEE Trans. Antennas Propag. **13**, 410–422 (1965).